Turbulent Flow Produced by Twin Slot Jets Impinging a Wall

Fatiha Bentarzi[1] and Amina Mataoui[1, *]

Abstract: The dynamics of two fully developed turbulent jets, perpendicular to a heated flat plate and related heat transfer mechanism are analysed numerically. This problem is relevant to several thermal engineering applications. The governing equations are solved by a finite volume method with a second order RSM model combined with wall functions used for turbulent modelling. The possibility to improve heat transfer is assessed taking into account the characteristic parameters for the jet-wall interaction. In particular, a parametric study is conducted by varying the jet Reynolds number (Re) and the nozzle to plate distance (D). The distance between the two jets (H) is set to 20 times the nozzle thicknesses (w). The results show the presence of a complex scarf vortex formed around each impinging jet, and a fountain-up wash flow resulting from the interaction of the jet with the wall. Though an increase in the Reynolds number has a weak effect on the overall flow structure, it produces a systematic rise of Nusselt number. The maximum heat transfer is reached at the stagnation points (dynamics similar to those already known for a single jet). The influence of the non-dimensional parameter (D/w) on the Nusselt number, however, is significant. The maximum local heat exchange between the wall and the flow occurs when the wall is located at the end of the potential core (D=6 w). The average Nusselt number is correlated with the Reynolds number, for two ranges of impinging distances (wall located before and after the potential core end).

Keywords: Twin impinging jets, heat transfer, turbulence, CFD, fountain flow.

Nomenclature

Latin symbols

Cp	Pressure coefficient, (-)
D	Distance between the jet exit to the wall, (*m*)
H	Distance between the two jets, (*m*)
k	Turbulent kinetic energy, ($m^2\,s^{-2}$)
L	Wall length, (*m*)
Nu	Nusselt number, (-)
Pr	Prandlt number, (-)

[1] Theoretical and applied laboratory of fluid mechanics, Physics Faculty, University of Science and Technology Houari Boumediene-USTHB, Algiers, Algeria.

[*] Corresponding Author: Amina Mataoui. Email: amataoui@usthb.dz.

Pr_t	Turbulent Prandtl number, (-)
Re	Reynolds number, (-)
T	Mean temperature, (K)
T_w	Wall temperature, (K)
T_0	Ambient temperature, (K)
U_i	Velocities components, ($m\ s^{-1}$)
U_0	Jet exit velocity, ($m\ s^{-1}$)
U_c	Mean longitudinal velocity on the x-axis, ($m\ s^{-1}$)
U_{max}	*M*aximum mean velocity, ($m\ s^{-1}$)
x_i	Point coordinate, (m)
X_{MP}	Merging point location, (m)
X_{CP}	Combining point location, (m)
w	Nozzle thickness, (m)

GreekSymbols

ε	Dissipation rate of turbulent energy, ($m^2\ s^{-3}$)
ν	Viscosity kinematic, ($m^2\ s^{-1}$)
ν_t	Eddy viscosity, ($m^2\ s^{-1}$)
ρ	Fluid density, ($kg\ m^{-3}$)

1 Introduction

In the last decades, heat transfer in jet impingement has received extensive attention in many industrial and engineering applications (e.g. manufacturing, material processing, electronic cooling, drying paper or textiles, tempering of glass, etc.). This has been due to the high heat transfer rates of jet impingement. A turbulent jet impinging normally on a flat plate is a very effective means to promote high rates of heat exchange. Different types of interactions occur when the wall is located before, within and after the merging region of the twin jets. A number of comprehensive reviews of jet impingement are available in the literature review of Zuckerman et al. [Zuckerman and Lior (2006)] as well as Shukla et al. [Shukla and Dewan (2017)]. Flow and thermal characteristics of jet impingement: comprehensive review. Relevant studies in the field of impingement of a confined jet issuing impinging normally a heated wall have been conducted by many researchers, as Jones et al. [Jones and Launder (1972); Launder and Spalding (1974); Cooper, Jackson, Launder et al. (1993); Benmouhoub and Mataoui (2013); Iachachene, Matoui and Halouane (2014); Lam and Prakash (2017)]. In most applications, a turbulent jet of gas or liquid is directed to the target area. San et al. [San and Lai (2001)] have examined the effect of jet-to-jet spacing on local Nusselt number for confined circular air jets vertically impinging on a flat plate. Narayanan et al. [Narayanan, Seyed-Yagoobi and Page (2004)] have carried out an experimental study of fluid mechanics and heat transfer in an impinging slot jet flow. Two nozzle-to-surface ratios of 3.5 and 0.5, which correspond to transitional

and potential-core jet impingement, are considered. Rady et al. [Rady and Arquis (2006)] examined heat transfer enhancement of multiple impinging slot jets. A Numerical analysis of the heat transfer due to confined slot-jet impingement on a moving plate was detailed by Sharif et al. [Sharif and Banerjee (2009); Benmouhoub and Mataoui (2014)]. The analysis reveals that the average Nusselt number increases considerably with the jet exit Reynolds number as well as with the plate velocity.

The present paper reports computations of the flow and thermal fields for two plane isothermal fully developed turbulent jets, perpendicular to a heated flat plate. Reynolds stress model was used for turbulence modelling. This configuration has been involved in several works for its interesting applications in heat transfer phenomena. The influences of nozzle to plate distance within the merging region, and Reynolds number on flow field and heat transfer are examined.

2 Mathematical formulation

Two identical jets issuing from nearby nozzles, into still surrounding are called, in the literature, "twin jets" or "dual jets". The entrainment of surrounding fluid from the jet boundaries causes a sub atmospheric region between jets. Because of the negative pressure region, the jets trajectories attract towards each other.
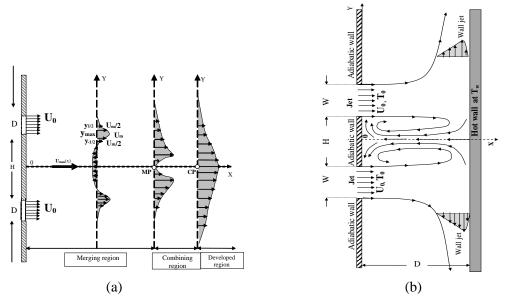

Figure 1: Flow characteristics (a) Twin free jet interaction (b) Twin jet impinging a wall

Consequently, the two jets converge and merge together to compose a single jet. Twin jets flow field is characterized by three distinct regions as converging region, merging region and combined region. The schematic of the flow field of free twin jet interaction is given in Fig. 1(a). Two converging jets, deflected by the sub atmospheric region between them, approach the plane of symmetry with increasing distance x from the nozzle exit. At the end of the converging region, jets merge at X_{MP}. The merging point is determined by the stagnation point where the mean velocity is zero in the symmetry axis x. The longitudinal mean velocities

have positive direction downstream of the merging point and negative direction. This work one considers the case of impinging flat heated plate in Fig. 1(b).

It is assumed that the turbulent air flow, having a velocity U_0 and a temperature T_0, is fully developed at each nozzle exit. The most important parameters of this problem are the jet exit velocity U_0, the thickness of the nozzle w of 1 cm, the distance between the nozzles to plate D, generally expressed in the dimensionless form D/w and the separating distance between the two nozzles is H=20 w in Fig. 1(b). The impingement surface is a hot flat plate at a constant temperature over its entire length "L". It is important to note that convection is approximated to be the only form of heat transfer in this study. While this might not entirely be the case, others have shown that the heat loss due to conduction and radiation makes up only a small percent of the total heat loss.

2.1 Governing equations

Mass conservation equation (Eq. 1), conservation of averaged momentum equation (Eq. 2) and the averaged energy equation (Eq. 3) of the turbulent incompressible flows are written as follow:

Mass conservative equation

$$\frac{\partial U_i}{\partial x_i} = 0 \tag{1}$$

Momentum conservation equation

$$\rho U_j \frac{\partial U_i}{\partial x_j} = -\frac{\partial P}{\partial x_i} + \frac{\partial}{\partial x_j}\left(\mu \frac{\partial U_i}{\partial x_j} - \rho \overline{u_i u_j}\right) \tag{2}$$

Energy conservation equation

$$\rho U_i \frac{\partial T}{\partial x_i} = \frac{\partial}{\partial x_i}\left(\frac{\mu}{p_r}\frac{\partial T}{\partial x_i} - \rho \overline{u_i \theta}\right) \tag{3}$$

Where P, T and U_i are the mean pressure, temperature and velocity components respectively, θ and u_i are the fluctuating temperature and velocity components, respectively. x_i is the coordinate direction, and ρ, μ are the fluid density and dynamic viscosity respectively.

2.2 Turbulence modeling

The closure of the averaged equations is achieved by linear strain pressure-Reynolds stress second order model. This model does not require eddy viscosity hypothesis. Six transport equations of each Reynolds stresses components ($\rho\overline{u_i u_j}$) are combined to RANS equations. The standard Reynolds stress model based on dissipation equation ε [Launder, Reece and Rodi (1975)] is expressed by:

$$\frac{\partial}{\partial x_m}(\rho U_m \overline{u_i u_j}) - \frac{\partial}{\partial x_m}\left(\left(\delta_{ml}\mu + C_s\rho\frac{k}{\varepsilon}\right)\frac{\partial(\overline{u_i u_j})}{\partial x_l}\right) = Pij - \frac{2}{3}\delta_{ij}\rho\varepsilon + \Phi_{ij} \tag{4}$$

Where *Pij*, the production term is given by (Eq. 5)

$$Pij = \rho \overline{u_i u_k} \frac{\partial U_j}{\partial x_k} - \rho \overline{u_j u_k} \frac{\partial U_i}{\partial x_k}$$
(5)

Φij is the pressure strain correlation. This term can be separated into two parts as:

$$\Phi_{ij} = \Phi_{ij,1} + \Phi_{ij,2}$$
(6)

Where $\Phi_{ij,1}$ is the 'slow' term, also known as the return-to-isotropy term, and $\Phi_{ij,2}$ is called the 'rapid' term. As the turbulence dissipation appears in the individual stress equations, an equation for ε is then required. This later is given by:

$$\frac{\partial(\rho U_m \varepsilon)}{\partial x_m} = \frac{\varepsilon}{k}(C_{\varepsilon 1} P_k - C_{\varepsilon 2} \rho \varepsilon) + \frac{\partial}{\partial x_m}\left[\left(\mu \delta_{ml} + C_\varepsilon \rho \frac{\varepsilon}{k} \overline{u_k u_l}\right)\frac{\partial \varepsilon}{\partial x_l}\right]$$
(7)

$$P_k = -\rho \overline{u_i u_j} \frac{\partial U_i}{\partial x_j}$$
(8)

In this study, the production due to the buoyancy is neglected, and the SSG model developed by Speziale et al. [Speziale, Sarkar and Gatski (1991)], using a quadratic relation for the pressure-strain correlation is utilized. The pressure-strain correlations have the following form that depends on the anisotropy tensor a_{ij}, the mean strain rate tensor S_{ij} and vorticity tensor Ω_{ij}.

$$\Phi_{ij,1} = -\rho \varepsilon \left[C_{S1} a_{ij} + C_{S2}\left(a_{ik} a_{kj} - \frac{1}{3} a_{mn} a_{mn} \delta_{ij}\right)\right]$$
(9)

$$\Phi_{ij,2} = -C_{r1} P a_{ij} + C_{r2} \rho k S_{ij} + C_{r3} \rho k S_{ij} \sqrt{a_{mn} a_{mn}} + C_{r4} \rho k \left(a_{ik} S_{jk} + a_{jk} S_{ik} - \frac{2}{3} a_{kl} S_{kl} \delta_{ij}\right)$$
(10)

$$+ C_{r5} \rho k \left(a_{ik} \Omega_{jk} + a_{jk} \Omega_{ik}\right)$$

Where

$$a_{ij} = \frac{\overline{u_i u_j}}{k} - \frac{2}{3}\delta_{ij}$$

$$S_{ij} = \frac{1}{2}\left(\frac{\partial u_i}{\partial x_j} + \frac{\partial u_j}{\partial x_i}\right)$$

$$\Omega_{ij} = \frac{1}{2}\left(\frac{\partial u_i}{\partial x_j} - \frac{\partial u_j}{\partial x_i}\right)$$

The constants of this model are given in Tab. 1.

Table 1: Reynolds stress constant model

C_{s1}	C_{s2}	C_{r1}	C_{r2}	C_{r3}	C_{r4}	C_{r5}
1.7	-1.05	0.9	0.8	0.65	0.625	0.2

Turbulent heat fluxes $\overline{\rho u_i \theta}$ necessitate also modeling. By analogy with molecular transport, in this study, the Simple Gradient Diffusion Hypothesis (SGDH) is used. The velocity-temperature correlations are deduced from the following algebraic equations which are also based on the Boussinesq hypothesis:

$$\overline{u_j \theta} = \Gamma_t \frac{\partial T}{\partial x_j} \quad \text{Where} \quad \Gamma_t = \frac{v_t}{Pr_t} \tag{11}$$

v_t Is the turbulent viscosity given by Prandtl-Kolmogrov equation:

$$v_t = C_\mu \frac{k^2}{\varepsilon} \tag{12}$$

Rather significant viscosity effects characterize the flow close to the wall. Therefore, the high Reynolds models are no longer suitable any more in this area of flow. The wall treatment is required. After several tests, the enhanced wall treatment predicts the flow fields with the best accuracy [Kader (1981)].

2.3 Numerical procedure

The governing equations for the mean values and turbulent quantities are solved using finite volume method on collocated meshes [Launder and Spalding (1974); Patankar (1980)]. This method requires a transformation of the equations in the general form which include convection, diffusion and source terms in the following form:

$$\frac{\partial}{\partial x_j} \left(\rho U_i \phi - \Gamma_\phi \frac{\partial \phi}{\partial x_j} \right) = S_\phi \tag{13}$$

Where may represent U_i, $\overline{u_i u_j}$, or T. The terms Γ_ϕ and S_ϕ are deduced for each variable Φ from their corresponding transport equations (Tab. 2).

For pressure-velocity coupling SIMPLE algorithm is used. The Power Law interpolation scheme is applied for the convection-diffusion term for all variables except the pressure where the second order scheme is used. As usual, the source terms in the turbulence equations are linearized to insure the stability of the solution.

The boundary conditions need to be specified on all surfaces of the computational domain. Boundaries presented in this study include inflow (Inlet), solid wall and outlet as follows:

-The inlet boundary conditions are given in Tab. 3

-On the solid wall, all mean and turbulent dynamical quantities are zero and the temperature is kept at T_w=360 K.

-The pressure is imposed to the atmospheric value at outlet boundary.

Table 2: Diffusion coefficients and source terms of RSM model

Equation	Φ	Γ_ϕ	S_ϕ
Continuity	1	0	0
Momentum	U_i	$\mu_{eff} = \mu_t + \mu$	$\left[-\dfrac{\partial p}{\partial x_i} + \dfrac{\partial}{\partial x_j}\left(\mu_{eff}\dfrac{\partial U_i}{\partial x_j} \right) \right]$
Energy	T	$\dfrac{\mu}{P_r} + \dfrac{\mu_t}{\mathrm{Pr}_T}$	0
Reynolds stresses	$\rho\overline{u_i u_j}$	$\mu\delta_{kl} + C_s\rho\dfrac{k}{\varepsilon}\overline{u_k u_l}$	$Pij - \dfrac{2}{3}\delta_{ij}\rho\varepsilon + \Phi_{ij}$
Dissipation rate	ε	$\mu\delta_{kl} + C_\varepsilon\rho\dfrac{\varepsilon}{k}\overline{u_k u_l}$	$\dfrac{\varepsilon}{k}\left(C_{\varepsilon 1}P_k - C_{\varepsilon 2}\rho\varepsilon \right)$

Table 3: Inlet boundary conditions at each jet exit

U	V	k	ε	T
U_0	0	$\dfrac{3}{2}(IU_0)^2$	$\dfrac{C_\mu^{3/4} k^{3/2}}{0.09w}$	T_0

2.4 Grid sensitivity analysis and validation

A non-uniform rectangular two dimensional grid is generated in this study. Structured meshes are used. Grids refinements are generated horizontally near the jet exit area and in the vicinity of the wall to take into account the viscous effects.

The typical grids of twin jet interaction (D/w=4) is illustrated in Fig. 2(a).

For example, for the case D/W=4, several grids are tested as shown in Fig. 2(b). This figure confirms that both Grids 4 and 5 give similar results. Therefore, in order to save computational time, Grid 4 is selected. Similar tests are done for each impinging distance. For the validation, we do not find experimental results for the case of a twin jet impinging a solid wall, for this we have validated this numerical method and turbulence model with the experimental results of single jet (Fig. 3). A good agreement is obtained with experimental data of Gardon et al. [Gardon and Akfirat (1966)] for the case of D/W=8 and Re=11000 (Fig. 3).
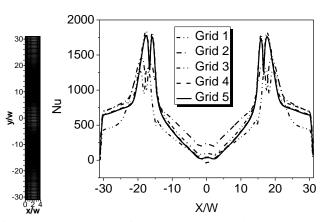
Figure 2: Grid of twin jet interaction for D/w=4. (a) Typical grid; (b) Grid test example Grid 1: 20000 nodes; Grid 2: 25000 nodes; Grid 3: 30000 nodes; Grid 4: 35000 nodes and Grid 5: 40000 nodes
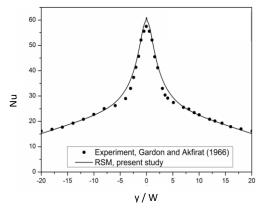

Figure 3: Validation of numerical procedure (D/w=8 and Re=11000)

3 Results and discussion

In this paper, several impinging fountain flows are studied. The parameters of this study are the jet Reynolds number (7000<Re<22,000), nozzle-to-impingement surface spacing (2<D/w<12), and nozzle-to-nozzle spacing is wide enough in order to examine merging region (H/W=20).

In the potential core the longitudinal velocity exceeds 95% of the jet exit velocity [Jambunathan, Lai, Moss et al. (1992)]. The length of the potential core strongly depends on the inlet conditions (velocity profiles and turbulence rate). It is found that this may area extend from 4-7, 7 nozzle thicknesses for the slot jet [Chan, Leung, Jambunathan et al. (2002)]. The impinging distances are selected such that for the smallest relative distance (D<4 w), the wall is set in the potential core region of each jet. For the second distance (D=6 w), the wall is set at the end of the potential core and for the 6 w<D<12 w, the wall is outside the potential core region. For all the studied cases, the wall is located in the merging region.

3.1 *Mean flow structure and isotherms distributions*

The calculated results show that the flow field structure of twin-jet impinging on a flat surface is strongly affected by the impinging distance (Fig. 4). Also, several recirculation zones are highlighted. In addition, fountain up wash flow is extended to the narrow region of the outer boundary.
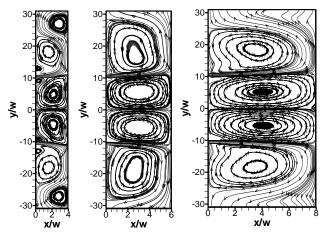

Figure 4: Streamlines contours for Re=11000

For all cases, the impingement of the jet on the walls produces the separation of the flow into two parts which are deflected in opposed direction. For a small impinging distance D<6 w, two further secondary eddies appear near the confining wall, at each side of the two jets. The deflection produces a high pressure zone at the wall.When the wall is located in the potential core of each jet exit (D/w<6), the big turbulent structure developed in the jet compresses the main eddying structure. As it can be seen, the primary vortices are close to the impinging wall. The penetration of the new recirculation area is highlighted by the secondary vortex within the confining wall area. Symmetrical flow structure is evidenced for all impinging distance. Calculated pressure contours are shown in Fig. 5 for three impinging distances. This figure makes clear the occurrence of positive high pressures at the impinging zones while low negative pressure zones appear in the region where the flows undergo strong curvature effects by 180º deflection (Coanda Effect).
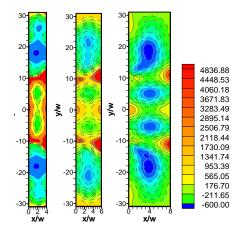
Figure 5: Isobars in Pa (Re=11000)

The cooling of the heated wall is deepened in this paper. The isotherms are illustrated in Fig. 6. As shown in this figure, the isotherms are closely affected by the behavior of the flow field (see the streamlines). This is expected because it is about a forced convection problem.
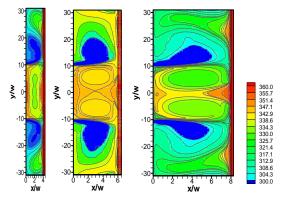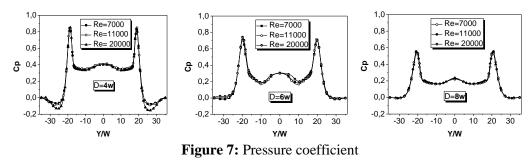

Figure 6: Isotherms contours in Kelvin

3.2 Effect of impinging distance on dimensionless parameters

The effect of the location of the wall is highlight by pressure coefficient and Nusselt number along the wall for several Reynolds numbers and impinging distances.

3.2.1 Pressure coefficient

Fig. 7 depicts a comparison of the static pressure distribution along the impinging wall for several impinging distances and Reynolds numbers. We notice that the pressure coefficients exhibit the same shape for each impinging distance. All curves have a symmetrical shape. The maximum corresponds to the location of the stagnation point and decreases when impinging distance augments. Beyond that, the pressure coefficient symmetrically decreases on both sides of each jet. For a small impact distance D=4 w, two apparent negative minima occur in front of the secondary vortices of the confining wall. For

a given impinging distance, the Reynolds number does not have any effect on pressure coefficient. At the open boundary (exit), atmospheric pressure is attained (Cp=0.0).

Figure 7: Pressure coefficient

3.2.2 Heat transfer coefficient evolution

The local Nusselt number along the impinging plate *Nu(y)* is calculated as follows:

$$Nu(y) = -\left(\frac{w}{T_H - T_C}\right)\left(\frac{\partial T}{\partial x}\right)_{x_{wall}} \tag{14}$$

Fig. 8 illustrates the evolution of the local Nusselt number along the hot wall, for various impinging distances and Reynolds number. The analysis of these curves allows the following conclusions:

The curves have a symmetrical shape. The maximum are observed at the stagnation point of the jet. Beyond that, the local Nusselt number symmetrically decreases on both sides of each jet. Furthermore this figure confirms that when the impinging distance decreases the heat transfer coefficient increases. In addition the increase of Reynolds number leads to an increase of the heat transfer. This evolution is completely expected because *Nu* is determined from the mean temperature gradient, while the mean temperature field is governed by a convection-diffusion equation. The stagnation points, in vicinity of the both sides of each twin peak, induce secondary peaks in Nusselt number distribution. Furthermore, we notice, at the locations of secondary Nusselt maxima, the pressures coefficient have negative minimum values in the sub atmospheric regions.

The comparison of the results of flow structure and heat transfer, it is seen that there is a relation between the sub atmospheric regions in pressure distributions and secondary peaks in heat transfer coefficients on the impingement plate.

The distribution of the local Nusselt number of the single jet is very different from that of the two jets impinging a hot wall. We note for the case D/w=8 (Fig. 3), a maximum pronounced at the axis of symmetry; in contrast for the case of two jet there is 4 obvious peaks in vicinity of the both sides of each jet, and at the symmetry axis a minimum of very small value (almost zero).
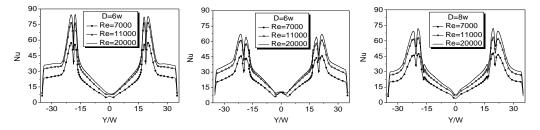
Figure 8: Effect of Reynolds number on Local Nusselt number for several impinging distances

The average Nusselt number along the heated wall is deduced from Eq. (15):

$$\overline{Nu}_{wall} = \frac{1}{L} \int_{-\frac{l}{2}}^{+\frac{l}{2}} Nu \; dl \tag{15}$$

Fig. 9 shows the effect of both impinging distance and Reynolds number, on heat transfer through the value of average Nusselt number. Based on Fig. 9, the average Nusselt number is correlated according the parameters of this study: Reynolds number Re and two ranges of impinging distance *D*:

When the plate is located before the potential core:

$$H = 20w, \; 2 \le D/W \le 6; \quad \overline{Nu} = 0,02 \left(D/w\right)^{0,86} Re^{0,69} \tag{16}$$

When the plate is located outside the potential core:

$$H = 20w, \; 6 < D/W \le 12; \quad \overline{Nu} = (0,413 - 0,06 \left(D/w\right) + 0,003 \left(D/w\right)^2) Re^{0,656} \tag{17}$$
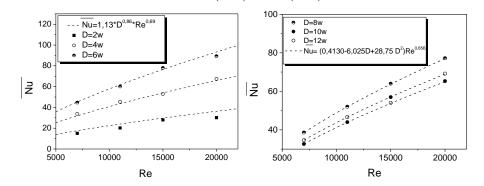

Figure 12: Effect of Reynolds number on average Nusselt number for several impinging distances

4 Conclusions

The interaction of twin turbulent jet with a hot wall is investigated numerically using the Reynolds Stress Model (*RSM*). The effects of Reynolds number and impinging distance on the flow fields and heat transfer are deepened. In the range of Reynolds number investigated in this paper, an increase of Reynolds number has a minor effect on the overall flow structure but produces a systematic rise of Nusselt number. For a small impinging distance D<4 w, two apparent negative minima of pressure coefficient occur in front of the

secondary vortices of the confining wall. For a given impinging distance, the Reynolds number does not have any effect on pressure coefficient. The maximum heat transfer is obtained at the stagnation points. The same phenomena as single jet was observed and maximum Nusselt number take place at the stagnation points at the impingement points of the jets. The maximum local heat exchange between the wall and the flow occurs for D=6 w. Two correlations of average Nusselt number along the hot wall are proposed for two ranges of impinging distances ($\overline{Nu} = f(\text{Re}, D/w)$).

References

Benmouhoub, D.; Mataoui, A. (2013): Turbulent heat transfer from a slot jet impinging on a flat plate. *Journal of Heat Transfer*, vol. 135, no. 10.

Benmouhoub, D.; Mataoui, A. (2014): Inclined plane jet impinging a moving heated wall. *Fluid Dynamics & Materials Processing*, vol. 10, no. 2, pp. 241-260.

Chan, T. L.; Leung, C. W.; Jambunathan, K.; Ashforth-Frost, S.; Zhou, Y. et al. (2002): Heat transfer characteristics of a slot jet impinging on a semi-circular convex surface. *International Journal of Heat and Mass Transfer*, vol. 45, no. 5, pp. 993-1006.

Choi, M.; Yoo, H. S.; Yang, G.; Lee, J. S.; Sohn, D. K. (2000): Measurements of impinging jet flow and heat transfer on a semi-circular concave surface. *International Journal of Heat and Mass Transfer*, vol. 43, no. 10, pp. 1811-1822.

Cooper, D.; Jackson, D. C.; Launder, B. E.; Liao, G. X. (1993): Impinging jet studies for turbulence model assessment-I. Flow-field experiments. *International Journal of Heat and Mass Transfer*, vol. 36, no. 10, pp. 2675-2684.

Gardon, R.; Akfirat, J. C. (1966): Heat transfer characteristics of impinging two-dimensional air jets. *Journal of Heat Transfer*, vol. 88, no. 1, pp. 101-107.

Iachachene, F.; Matoui, A.; Halouane, Y. (2014): Heat transfer related to a self-sustained oscillating plane jet flowing inside a rectangular cavity. *Fluid Dynamics & Materials Processing*, vol. 10, no. 4, pp. 503-520.

Jones, W. P.; Launder, B. E. (1972): The prediction of laminarization with a two equations model of turbulence. *International Journal of Heat and Mass Transfer*, vol. 15, pp. 301-314.

Jambunathan, K.; Lai, E.; Moss, M. A.; Button, B. L. (1992): A review of heat transfer data for single circular jet impingement. *International Journal of Heat and Fluid Flow*, vol. 13, no. 2, pp. 106-115.

Kader, B. A. (1981): Temperature and concentration profiles in fully turbulent boundary layers. *International Journal of Heat and Mass Transfer*, vol. 24, no. 9, pp. 1541-1544.

Lam, P. A. K.; Prakash, K. A. (2017): A numerical investigation and design optimization of impingement cooling system with an array of air jets. *International Journal of Heat and Mass Transfer*, vol. 108, pp. 880-900.

Launder, B. E.; Reece, G. J.; Rodi, W. (1975): Progress in the development of a Reynolds-stress turbulence closure. *Journal of Fluid Mechanics*, vol. 68, no. 3, pp. 537-566.

Launder, B. E.; Spalding, D. B. (1974): The numerical of computation of turbulent flows. *Computer Methods in Applied Mechanics and Engineering*, vol. 3, PP. 269-289.

Narayanan, V.; Seyed-Yagoobi, J.; Page, R. H. (2004): An experimental study of fluid mechanics and heat transfer in an impinging slot jet flow. *International Journal of Heat and Mass Transfer*, vol. 47, no. 8-9, pp. 1827-1845.

Patankar, S. (1980): *Numerical heat transfer and fluid flow, Series in Computational methods in mechanics and thermal sciences*. Hemisphere Publishing Corpration and Mc Graw Hill.

Rady, M.; Arquis, E. (2006): Heat transfer enhancement of multiple impinging slot jets with symmetric exhaust ports and confinement surface protrusions. *Applied Thermal Engineering*, vol. 26, no. 11-12, pp. 1310-1319.

San, J. Y.; Lai, M. D. (2001): Optimum jet-to-jet spacing of heat transfer for staggered arrays of impinging air jets. *International Journal of Heat and Mass Transfer*, vol. 44, no. 21, pp. 3997-4007.

Sharif, M. A. R.; Banerjee, A. (2009): Numerical analysis of heat transfer due to confined slot-jet impingement on a moving plate. *Applied Thermal Engineering*, vol. 29, no. 2-3, pp. 532-540.

Shukla, A. K.; Dewan, A. (2017): Flow and thermal characteristics of jet impingement: Comprehensive review. *International Journal of Heat and Technology*, vol. 35, no. 1, pp. 153-166.

Speziale, C. G.; Sarkar, S.; Gatski, T. B. (1991): Modelling the pressure-strain correlation of turbulence: An invariant dynamical systems approach. *Journal of Fluid Mechanics*, vol. 227, pp. 245-272.

Zuckerman, N.; Lior, N. (2006): Jet impingement heat transfer: physics, correlations, and numerical modeling. *Advances in Heat Transfer*, vol. 39, pp. 565-631.